Catalysis Letters (2019) 149:3349–3360
https://doi.org/10.1007/s10562-019-02883-8

Design of Co, Cu and Fe–BEA Zeolite Catalysts for Selective Conversion of Lactic Acid into Acrylic Acid

Natalia Sobuś[1] · Barbara Michorczyk[1] · Marcin Piotrowski[1] · Łukasz Kuterasiński[2] · Damian K. Chlebda[3] · Joanna Łojewska[3] · Roman J. Jędrzejczyk[4] · Przemysław Jodłowski[1] · Piotr Kuśtrowski[3] · Izabela Czekaj[1]

Received: 22 March 2019 / Accepted: 25 June 2019 / Published online: 19 July 2019
© The Author(s) 2019

Abstract

Design of the catalytic properties and structure of zeolite materials play a key role in efficient transformation of biomass to sustainable chemicals. In the present study, we have designed theoretical and experimental approach for the production of acrylic acid (AA) from lactic acid (LA) over zeolite catalysts. Various BEA zeolites modified with metals (Co, Cu and Fe) were prepared using ion exchange and sonication methods. In the theoretical studies the metal M–O–M dimers have been found to be stable above oxygen bound with aluminium centers of BEA zeolite. The mechanism of direct LA dehydration over the Co–, Cu– and Fe–BEA zeolites has been proposed. Experimentally, the investigated catalysts trend in following byproduct formation: AA, propionic acid (PA), 2,3-pentanedione (2,3-PD) or acetaldehyde (AC). The best selectivity towards acrylic acid was achieved in the presence of the Co– and Cu–BEA catalysts prepared by the sonication method.

Graphic Abstract

Direct lactic acid dehydration into acrylic acid over Co–, Cu– and Fe–BEA zeolites.

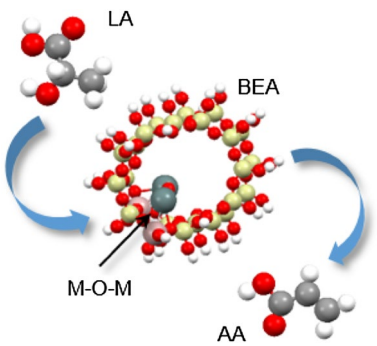

Keywords Lactic acid · Acrylic acid · Zeolite catalysts · Dehydration · Sonication

✉ Izabela Czekaj
iczekaj@chemia.pk.edu.pl

[1] Faculty of Chemical Engineering anf Technology, Cracow University of Technology, Warszawska 24, 31-155 Kraków, Poland

[2] Jerzy Haber Institute of Catalysis and Surface Chemistry, Polish Academy of Sciences, Niezapominajek 8, 30-239 Kraków, Poland

[3] Faculty of Chemistry, Jagiellonian University, Gronostajowa 2, 30-387 Kraków, Poland

[4] Malopolska Centre of Biotechnology, Gronostajowa 7A, 30-387 Kraków, Poland

1 Introduction

Nowadays crude oil and natural gas are the main sources for the production of fuels and feedstock chemicals. These resources are limited and the application of (renewable) alternatives will be needed in future to sustain the progress of mankind. The major challenge of society research is to build fuels and chemical intermediates from available and renewable materials that do not compete with food crops for cultivation areas, water or fertilizer [1]. Biomass, obtained for example from woody plant materials (e.g., corn and

wood wastes, grass etc.), is the one exceptional biorenewable feedstock for chemicals and fuels production [2, 3]. However, the use of biomass requires a sequence of chemical conversions, which is blocked by the main building carbohydrates. Recently, global efforts are underway to convert plant cell walls (which are collectively called lignocellulosic biomass) to biofuels for transportation needs [4–6]. Dehydration of lactic acid (LA) provides the most promising and environmentally friendly way to produce for example acrylic acid (AA). However, dehydration of LA may be accompanied by other competing reactions, such as hydrogenation, condensation, decarboxylation and esterification. The decarboxylation of LA to acetaldehyde is one of the major side reactions and has a large effect on the low selectivity to AA. To inhibit the formation of acetaldehyde and improve the selectivity to the desired AA, the effects of many different catalysts were tested.

LA has three available atoms for adsorption: the oxygen atom of the alcohol group and the two oxygen atoms of the carboxyl group. Based on the literature [7], the LA adsorption over metallic cations gives several possible binding modes at zirconia surfaces: monodentate, bidentate bridging and bidentate chelating, where a dissociative bidentate bridging mode is preferred. The classical pathway based on a carbocation formation proceeds with a very high activation energy. Therefore, the authors suggested another mechanism involving carbanions and succeeded with the AA formation. From all family of biomass derived compounds, LA is the most promising and can generate multiple final and intermediate chemicals, such as AA, pyruvic acid, 1,2-propanediol, 2,3-pentanedione or acetaldehyde [8, 9]. This compound can also be polymerized into biodegradable plastic, i.e. polylactide (PLA), or solvents. AA is one of the most important for the synthesis of organic compounds. It is widely used for the preparation of a variety of materials, such as water absorbent polymers, adhesives, and textile treating agents. The most common industrial process for preparing AA is the selective oxidation of propylene, using a two-step process (Fig. 2). This is the basic method of obtaining the product in the fossil industry. However, it is widely affected by the propylene price as it represents only 2% of its global consumption [10]. The value of the AA market in 2013 year was equal 11 billion $ yearly and the forecast until 2020 is around 18.8 billion $. In next 5 years, the global demand for AA will be around 8.169 billion tons/year. Due to the high demand for fossil fuels and the relative low stocks of crude oil, the prices of propylene and its by-products grow, leading to increased pressure on the production of AA from propylene. AA is a platform molecule used as a building block to produce acrylate polymers and plastics [10]. Its production had grown 4% per year between 2006 and 2011 reaching 4.2 Mton in 2011 and was predicted to increase about 5% per year between 2012 and 2017. Recently, its production has reached a level of about 4.7 Mton/year [11]. An alternative route to produce AA is therefore required, especially in the context of commitment to environment friendly catalytic processes, for example a single step dehydration of LA. Catalytic dehydration of LA to AA has received increasing attention in the last two decades, but high selectivity has proven elusive. Metal exchanged zeolites are promising catalysts for the further development for the LA to AA dehydration. However, AA is rarely obtained selectively from LA, because of easy decarbonylation/decarboxylation leading to acetaldehyde and CO_x. High yields of AA were obtained using modified zeolites, but they suffered from coking and hydrothermal instability. Zeolites are very promising materials for biomass conversion into lactates, acrylates and may be used to obtain also other valuable products derived from biomass. [9, 12] Zeolites, microporous and crystalline aluminosilicates, are effective catalysts in many applications [8].

Huang et al. [13–16] studied the LA dehydration process on NaY zeolites, modified by rare earth metals (lanthanum, cerium, samarium and europium) from which La–NaY had the best selectivity to AA affording 50%. However, a challenge to develop an efficient zeolite catalyst with both high LA conversion and high AA selectivity still remains. Metal exchanged zeolites typically used for other processes could be an interesting class of catalysts for the LA dehydration reaction. One of the promising metals is Sn used in oxidation and reduction processes, or Fe, Co, Cu used recently in the DeNOx process [17].

J. Pérez-Ramírez et al. [18] also studied the LA dehydration process using hierarchical NaY zeolite, which exhibited a high selectivity to AA (75%). Important issues on the dehydration of LA were also presented by T. Bonnotte et al. [19].

The distribution of metal particles inside a zeolite structure has an essential role in catalytic processes and strongly depends on a method used for preparation of zeolite [20]. Therefore, it is important to understand structure of metal particles inside zeolite framework and their role in. One of the major obstacles to an improved understanding is the difficulty in modelling the complex and non-periodic structure of zeolites. Several groups were tackled zeolite crystal structure and model adsorption processes using both cluster and periodic DFT calculations [21–27]. However, more detailed studies on the structure of active sites and metallic nanoparticles carried in zeolites as well as mechanism of biomass conversion into chemicals are necessary.

Taking into account biomass valorization into valuable chemicals, in this study we are interested in designing a new theoretical and experimental approach for the synthesis of AA from LA over zeolite catalysts. The catalyst design using both experimental and theoretical methods should help in a

further development of effective technology for the biomass conversion.

2 Experimental Details

2.1 Catalyst Preparation

BEA zeolites were obtained in several steps. At the beginning, sodium aluminate (Riedel de Haën, p.a.) was dissolved in an aqueous solution of sodium hydroxide (Chempur, p.a.). Subsequently, a template, i.e. tetraethylammonium hydroxide (Sigma Aldrich, 40%), was added to the $NaOH/NaAlO_2$ solution. Finally, silica (Zeosil, 98%) was introduced under vigorous stirring to the resulting mixture. All prepared gels ($H_2O/SiO_2 = 12.5$; $NaOH/SiO_2 = 0.37$) were aged for 20 h. The aged gels were subsequently transferred into Teflon-lined stainless-steel autoclaves, sealed and kept at 150 °C for 72 h. The autoclaves were rotated at 56 rpm. After the synthesis the solids were centrifuged, washed and dried at 80 °C. In order to remove organic template calcination of the crystallized materials was carried out at 480 °C for 8 h with a temperature ramp of 2 °C/min. The BEA-type zeolites were prepared with Si/Al = 12–37. All samples were ion exchanged twice with a 0.1 M aqueous ammonium nitrate solution at 80 °C for 2 h. The ion exchanged samples were centrifuged and washed three times with distilled water and dried at RT. Then, the samples were calcined at 450 °C for 8 h with a temperature ramp of 2 °C/min. In the final step, the obtained zeolite samples were ion exchanged or sonicated in cobalt, copper or iron precursors. In the ion exchanged method, the zeolite samples were immersed into a 0.5 M aqueous copper nitrate solution at 20 °C for 24 h. Then, the ion exchanged samples were centrifuged and washed three times with distilled water and dried. The obtained Cu containing zeolites were calcined at 500 °C for 4 h with a temperature ramp of 2 °C/min and flow rate of dry air = 50 ml/min. In the sonochemical preparation route, the zeolites were placed in 0.5 M aqueous cobalt, copper or iron nitrate solutions and sonicated for 20 min. Prior to the sonication, the samples were outgassed for 15 min using Ar (Linde, 99.5%) with a flow rate of 20 ml/min, and 1.5 ml of ethanol was added to each suspension. The ultrasound irradiation of zeolite samples in the metal nitrate precursors was performed using a QSonica S-4000 sonicator (Church Hill Rd, Newtown, CT, USA) equipped with a ½" diameter horn. The average power of sonication used was c.a. 60 W, and frequency was 20 kHz. The centrifugation, drying and calcination processes were performed as above. In both ion exchange or sonication preparation methods 1.5 g of zeolite was treated with 100 ml of aqueous Co, Cu or Fe salt solutions. The catalysts prepared in this study are listed in Table 1.

Table 1 Characteristics of zeolite catalysts

Catalysts	Si/Al	Preparation method	Sonication time, (h)	Sonication energy, (J)	Metal content wt%	S_{Lang}, (m^2/g)	V_{total} (cm^3/g)	V_{micro} (cm^3/g)	Brønsted acid sites (μmol/g_{cat})	Lewis acid sites (μmol/g_{cat})
Na/BEA	12.5	–	–	–	1.1	762	0.36	0.14	50	34
Na/BEA	37.5				1.2	868	0.65	0.21	28	36
Cu/BEA	12.5	Ion-exchange	–	–	2.18	730	0.60	0.17	141	499
Cu/BEA/s	12.5	Sonication	1	67.8	4.16	744	0.51	0.15	186	638
Cu/BEA	37.5	Ion-exchange	–	–	2.16	711	0.53	0.15	212	461
Cu/BEA/s	37.5	Sonication	1	67.8	4.15	737	0.46	0.14	191	634
Co/BEA	12.5	Ion-exchange	–	–	1.43	432	0.25	0.09	142	392
Co/BEA/s	12.5	Sonication	1	65.8	4.68	533	0.30	0.11	207	719
Co/BEA	37.5	Ion-exchange	–	–	1.39	440	0.28	0.12	130	554
Co/BEA/s	37.5	Sonication	1	65.8	4.72	542	0.34	0.15	92	744
Fe/BEA	37.5	Ion-exchange	–	–	2.26	743	0.47	0.16	134	264
Fe/BEA/s	37.5	Sonication	1	64.0	2.44	759	0.44	0.16	233	405

2.2 Characterization

Chemical analysis was carried out using a Thermo Scientific ICE3000 series AAS spectrometer in F-AAS mode. The external standard calibration method was used for a metal content determination. In situ UV/Vis analyses of prepared catalysts were performed using a AvaSpec-ULS2048 StarLine Versatile Fiber-optic Spectrometer (Avantes BV, Apeldoorn, The Netherlands) equipped with AvaLight-DHc Full-range Compact Light Source allowing for measurements in a range of 200–2500 nm. The spectra were recorded in situ using Praying Mantis High-Temperature Reaction Chamber (Harrick Scientific Co., Ossining, NY, USA) with a home-made stainless-steel dome equipped with a high-temperature reflection probe FCR-7UV400-2-ME-HTX (7 × 400 µm fibres, Avantes BV). The in situ UV–Vis analyses were performed under dehydrated conditions at 110°C with a constant 50 ml/min helium flow (AirProducts). X-ray powder diffraction (XRD) patterns were recorded with a PANalytical X'Pert PRO MPD diffractometer. The measurements were carried out with CuKα radiation at 40 kV and 30 mA. The scanning was conducted in a continuous mode over a 2θ range from 5° to 50° with 0.033° step. Raman spectra were collected using a µRaman confocal microscope (LabRAM HR, Horiba Jobinn Yvonne, France) equipped with a red laser He–Ne (633 nm). Before recording the spectra, the microscope was calibrated using a crystalline Si plate and with respect to the main band corresponding to the structure of Si at 520.7 cm^{-1}. Data were registered using long working distance objective of 50 × and diffraction grating 1800 lines per mm. The laser power falling on the sample was < 1 mW. The spectral resolution provided by such spectrometer configuration is about 2 cm^{-1}. FT-IR spectra were recorded using a Nicolet 6700 spectrometer (Thermo Scientific) with a MCT detector. The scanning range was 650–4000 cm^{-1} with resolution of 4 cm^{-1}, and 100 scans per each spectrum. Prior to the IR studies, samples were pressed into thin wafers and activated in vacuum at 450 °C for 1 h. CO or NH_3 (Air Products 99.5% and 99.3%, respectively) were used as adsorbates. Small doses of CO were adsorbed on the surface of sample at − 100 °C or at room temperature. The procedure of ammonia adsorption was carried out at 130 °C. Porosity of zeolites was investigated by low temperature nitrogen sorption, and surface area (S_{Lang}, Table 1) was determined using the Langmuir isotherm equation, which has physical meaning for microporous materials.

Temperature-programmed reduction (H_2-TPR) were carried out in a modified gas chromatograph equipped with a thermal conductivity detector (TCD) connected on-line with a quartz microreactor. In the H_2-TPR measurements, a purified mixture of N_2/H_2 (95/5 vol%, Air Liquide) served as a combined carrier and reducing gas at a total flow rate of 30 ml/min. A dry catalyst (100 mg) was preheated in the reactor in pure helium (99.999 vol%, Linde) at 650 °C for 30 min and then cooled to RT in a He stream. Subsequently, the N_2/H_2 flow was applied and the temperature was raised from RT to 700 °C at a rate of 10 °C min^{-1}.

The surface composition of samples was investigated with X-ray photoelectron spectroscopy (XPS) using a Prevac photoelectron spectrometer equipped with a hemispherical analyzer (VG SCIENTA R3000). The spectra were taken using a monochromatized aluminum source Al Kα (E = 1486.6 eV). The base pressure in the analytical chamber was 5×10^{-9} mbar. The scale of the binding energy value was adjusted to the C 1s reference peak at 284.8 eV. The composition and chemical state of sample surface were analyzed taking into account the areas and binding energies of O 1s, C 1s, Si 2p, Al 2p, Cu 2p, Co 2p and Fe 2p photoelectron peaks. The spectra were fitted using CasaXPS software.

2.3 Theoretical Modelling

The electronic structure of all clusters was calculated by ab initio density functional theory (DFT) methods (program StoBe) using the non-local generalized gradient corrected functionals according to Perdew, Burke, and Ernzerhof (RPBE), in order to account for electron exchange and correlation [28]. The stabilization of dimeric metal complexes, such as M–OH, HO–M–O–M–OH and M–O–M (where M = Co, Cu and Fe) in the BEA zeolites framework has been investigated. The adsorption energies of the adsorbates on the cluster were calculated as follows:

$E_{ad}(adsorbate/cluster\_) = E_{tot}(adsorbate/cluster) - E_{tot}(cluster) - E_{tot}(adsorbate)$, where E_{tot}(adsorbate/cluster) is the total energy of the adsorbate/cluster surface complex_, E_{tot}(cluster) and E_{tot}(adsorbate) are the total energies of pure cluster and the adsorbate, respectively. A double zeta valence polarization (DZVP) type was used for the orbital basis sets of Co, Cu and Fe (63321/531/311), Si (6321/521/1), Al (6321/521/1), O, C (621/41/1), and H (41). Auxiliary basis sets, such as (5,5;5,5) for Si, Sn and Fe, (4,3:4,3) for O, C, N, and (41) for H, were applied to fit the electron density and the exchange–correlation potential. Several clusters, which represent BEA zeolite, have been analyzed and finally the $Al_2Si_{22}O_{64}H_{32}$ cluster has been used in the LA dehydration reaction. Figure 1 shows dimeric complex M–O–M (where M = Co, Cu or Fe) in the $Al_2Si_{22}O_{64}H_{32}$ cluster, LA structure to visualize compatibility with metal dimer as well as LA adsorption above M–O–M inside the BEA cluster and AA desorption from M–O–M inside the BEA cluster.

2.4 Catalytic Tests

The dehydration of LA was carried out in a vertical fixed-bed quartz reactor and operated under atmospheric pressure

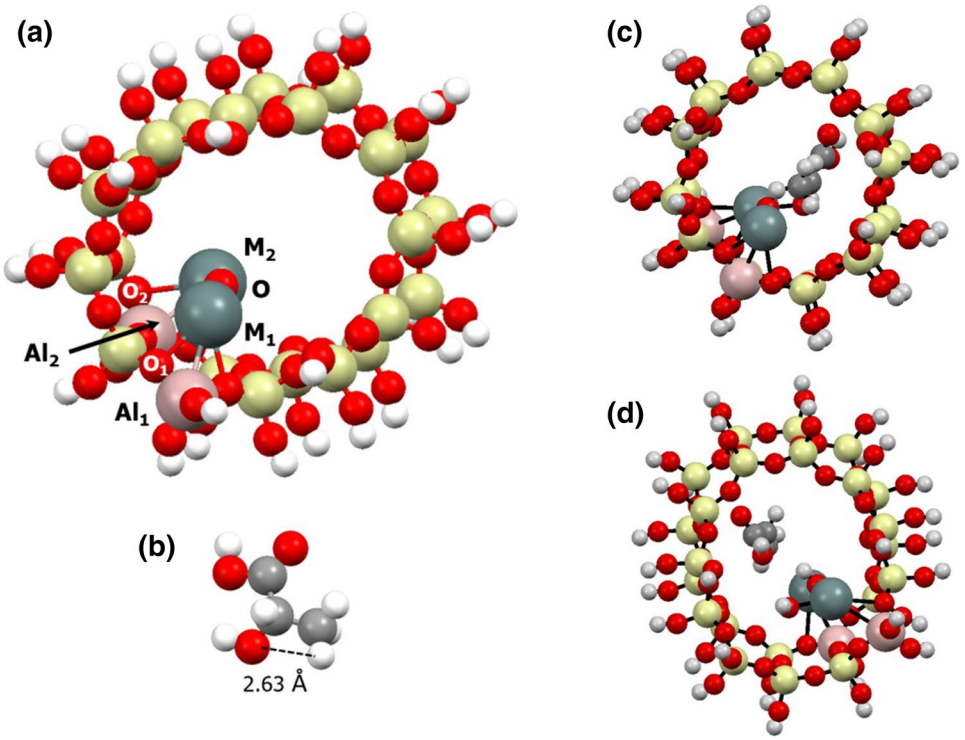

Fig. 1 **a** Dimeric complex M–O–M (where M = Co, Cu or Fe) in the BEA cluster, **b** lactic acid structure, **c** lactic acid adsorption above M–O–M inside BEA cluster, **d** acrylic acid desorption from M–O–M inside BEA cluster

at temperature of 370 °C. Figure 2 shows unit for catalytic tests in gaseous phase with all necessary lines. 0.25 g of a catalyst was diluted in SiC (0.5 g). The reaction feed, which was an aqueous solution containing 40 wt% LA, was pumped at a flow rate of 2 ml/h by an infusion pump into a mixer, where was evaporated at 150 °C, mixed with inert gas (He, 50 ml/min) and driven by the inert gas into the reactor. The liquid supernatant was analyzed using an Agilent 6890 N gas chromatograph (GC) with an BP21 FFAP capillary column (60 m, diameter 0.25 mm) and flame ionization detector (FID). The formation of AA was confirmed by a gas chromatography–mass spectrometer (GC–MS, with a DB-5MS capillary column: length 60 m, diameter 0.25 mm).

3 Results and Discussion

The goal of the study was to design an experimental approach for the synthesis of AA from LA over zeolite catalysts. Various BEA zeolites modified with metals (Co, Cu and Fe) were prepared using the ion exchange as well as

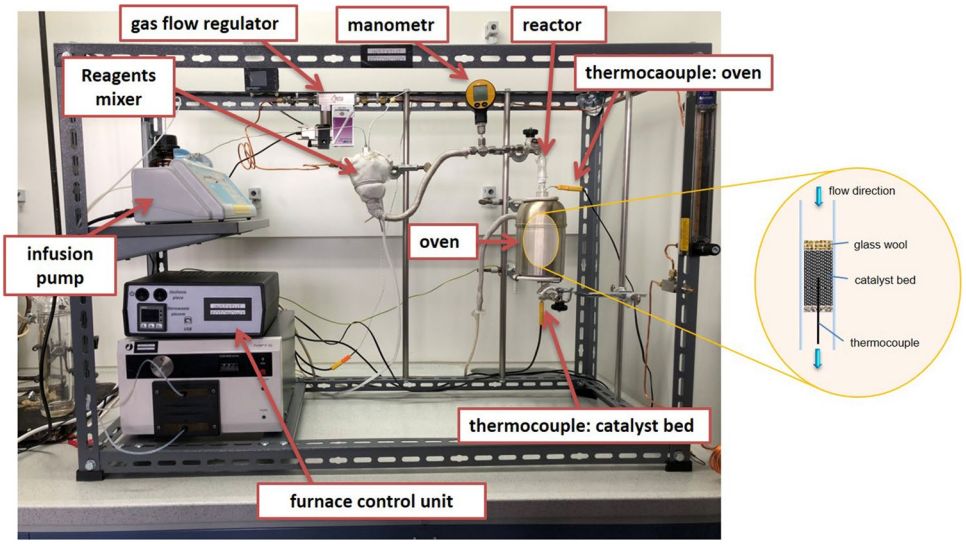

Fig. 2 Unit for catalytic tests in gaseous phase

sonication method. The catalysts preparation and characterization details are presented in Table 1.

To determine the possible coordination of prepared catalysts samples, the in situ DR UV–Vis measurements were performed. The results of in situ DR UV–Vis analyses for the Cu, Co and Fe-loaded catalysts are presented in Fig. 3a–c, respectively. The UV–Vis spectra of the Cu/BEA/s catalysts reveal the presence of monomeric Cu^{2+} and oligomeric [Cu^{2+}–O^{2-}–Cu^{2+}] species [29]. The additional band at 20000 cm^{-1} for the Cu/BEA samples may be attributed to Cu^{2+} in octahedral coordination. Moreover, the spectrum of the Cu-containing catalyst prepared using the sonochemical preparation method shows a decrease in intensity of bands related to monomeric species (25000 cm^{-1}) bands below 40000 and 35000 cm^{-1} which can be attributed to giving the rise to oligomeric species at 35000 cm^{-1} (Fig. 3).

The results of DR UV–Vis spectra for the Co containing samples are presented in Fig. 3. The catalysts prepared by the sonochemical methods exhibit characteristic bands at 40000, 26315 and 14925 cm^{-1} that can be attributed to the Co_3O_4 spinel structure. The spectrum of the Co/BEA catalyst prepared by the ion-exchange method reveals two bands at 20000 and 17200 cm^{-1} that may be attributed to $Co(H_2O)_6$ species in octahedral coordination and Co^{2+} species in tetrahedral coordination, respectively [30].

The DR UV–Vis spectrum of the Fe/BEA catalyst prepared by the sonochemical technique shows bands at: < 33333 cm^{-1}, 33333–25000 cm^{-1} and > 20000 cm^{-1}, which can be attributed to isolated Fe^{3+} in tetrahedral and higher coordination, oligomeric $Fe_x^{3+}O_y$ clusters located in zeolite pores and large Fe_2O_3 nanoparticles, respectively [31, 32]. It is worth mentioning that the band at 25000 cm^{-1} is well shaped confirming the presence of the formed nanoparticles.

The results of the XRD analyses are presented in Fig. 4. The comparison of the diffractograms of the prepared

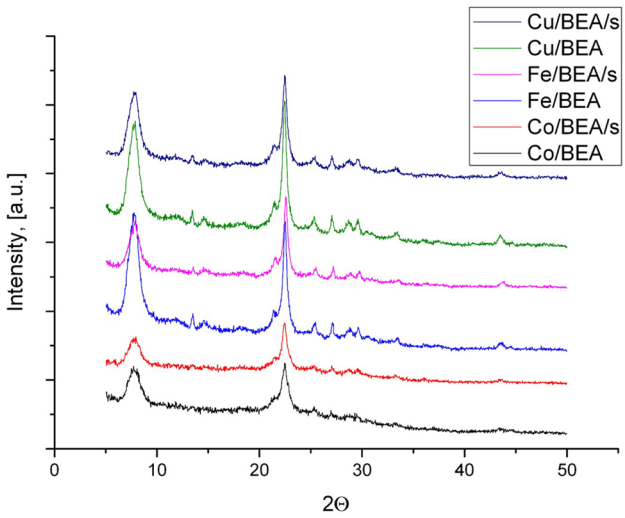

Fig. 4 XRD of prepared zeolites: Cu/BEA and Cu/BEA/s, Co/BEA and Co/BEA/s, Fe/BEA and Fe/BEA/s

zeolites with those available in International Zeolite Database confirms the presence of the specific BEA zeolite phase [33]. The obtained zeolite materials did not exhibit the presence of other crystalline phases. Additionally, it can be seen, that in the case of the catalysts prepared by the sonochemical route the crystalline structure remains unchanged.

The zeolite structure was also examined by Raman spectroscopy (Fig. 5). In addition to the bands of the zeolite skeleton (Fig. 5a, for comparison), [34, 35] a sharp band of 280 cm^{-1} and a weaker band at 604 cm^{-1} are observed, which suggest the presence of CuO [36, 37]. The spectrum of Co/BEA (shown in Fig. 5b) is difficult to interpret due to the high fluorescence of the sample, however, for the sonicated sample, five distinct bands can be distinguished at 190, 483, 520, 613 and 685 cm^{-1} corresponding to the Co_3O_4 spinel structure [38]. Concerning the Fe/BEA sample

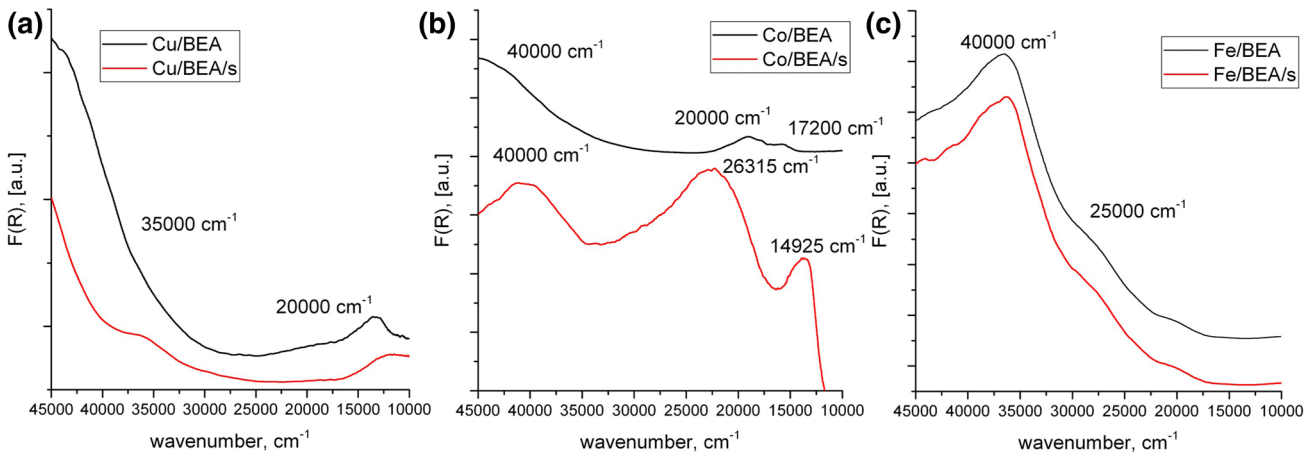

Fig. 3 UV–Vis spectra of prepared samples: **a** Cu/BEA and Cu/BEA/s. **b** Co/BEA and Co/BEA/s. **c** Fe/BEA/s

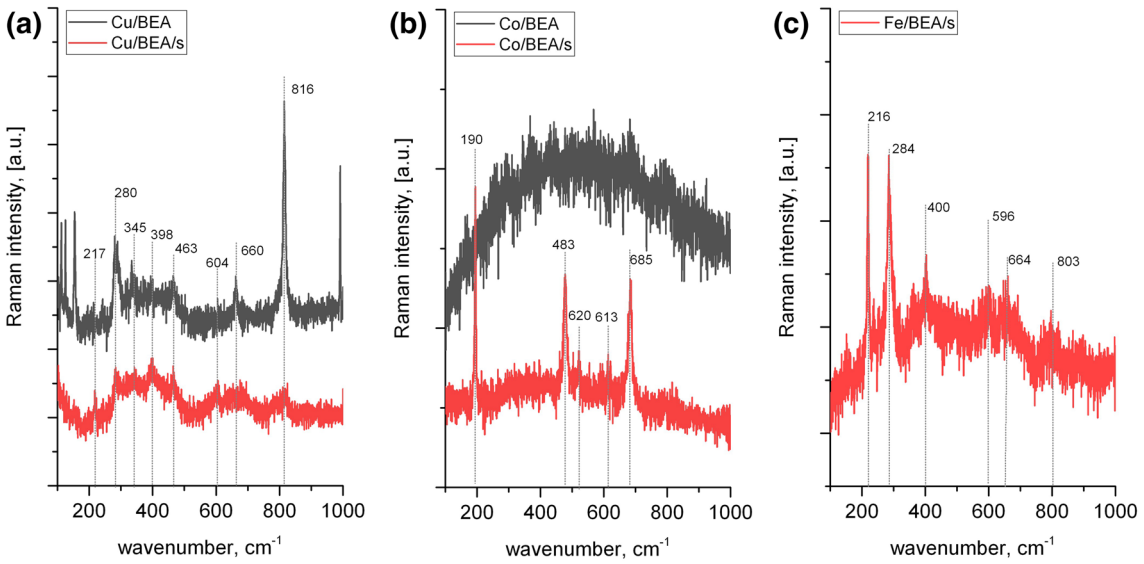

Fig. 5 Raman spectra of prepared samples: **a** Cu/BEA and Cu/BEA/s. **b** Co/BEA and Co/BEA/s. **c** Fe/BEA/s

(Fig. 5c) the spectrum indicates the bands originating from the hematite (α-Fe_2O_3) structure [39].

H_2-TPR profiles of the samples obtained by ion-exchange and sonication method are compared in Fig. 6. Two reduction maxima at 260 and 390 °C are observed on the TPR profile of copper-exchanged BEA (Cu/BEA). These maxima are assigned to multiple copper species reduction $Cu^{2+} \rightarrow Cu^{+}$. [40] In a contrast, over the Cu/BEA/s profile only one and sharp maximum at 260 °C appeared indicating clearly difference in reducibility of the Cu containing samples obtained by ion-exchange and sonication. In the case of the Co-containing BEA sample synthesized by ion-exchange two reduction maxima at 425 and 600 °C appeared. The peak at ca. 425 °C is typically assigned to CoO_x reduction (mainly Co^{2+} oxide species) while the maximum at 600 °C is ascribed to the slight reduction of Co^{2+} ions in the charge compensation sites to Co^{+} or Co^{0} [41]. In a contrast, on the TPR profile of the Co-containing sample produced by sonication three reduction peaks ca. at 350 °C, 370 °C and 455 °C appeared. These reduction maxima were assigned to the reduction of CoO_x occurring outside and inside the zeolite structure. [41, 42] The intensity of these reduction peaks were much greater than in the case of the sample obtained by ion-exchange indicating higher contribution of Co^{3+} oxide species. Moreover, in the case of the Co/BEA/s sample, above 600 °C any reduction accrued which may suggest

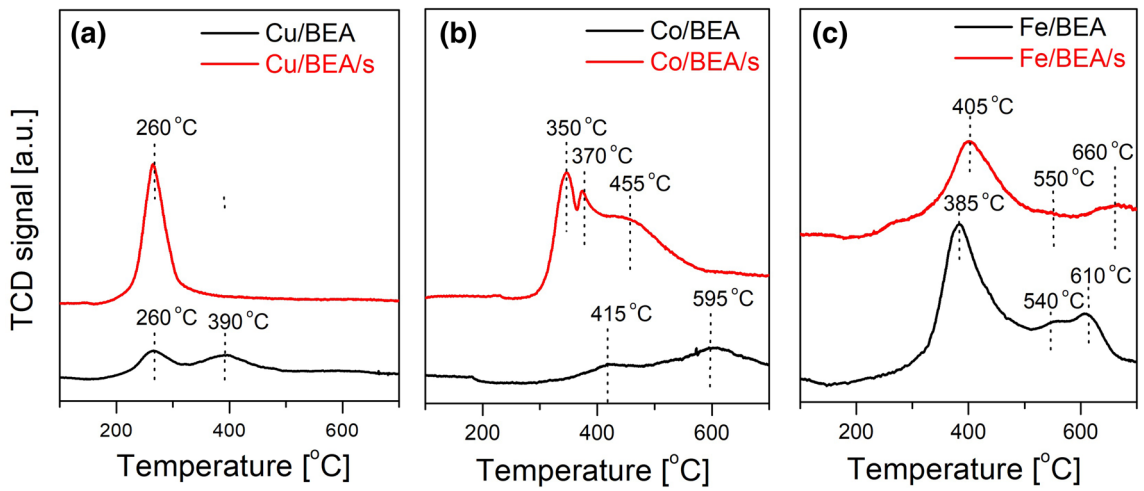

Fig. 6 H_2-TPR profiles of samples obtained by ion-exchange and sonication method: **a** Cu/BEA and Cu/BEA/s. **b** Co/BEA and Co/BEA/s. **c** Fe/BEA and Fe/BEA/s

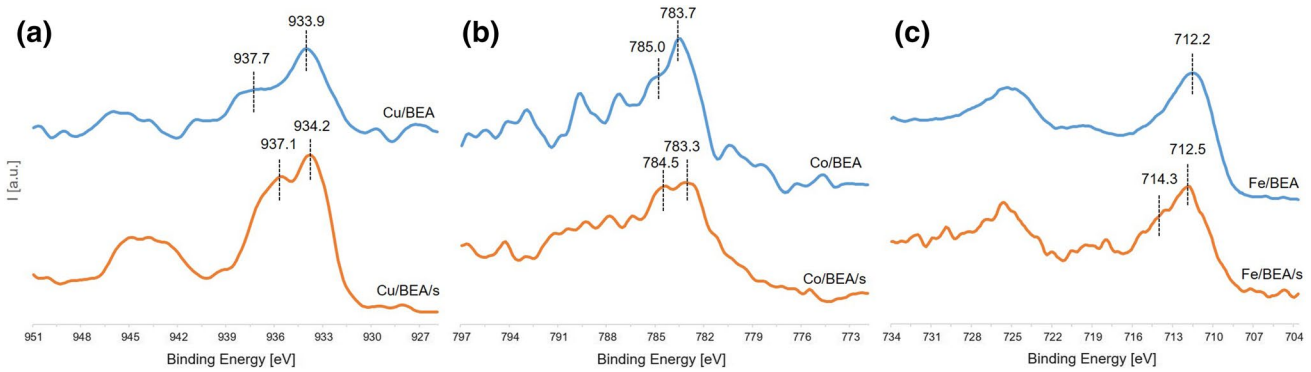

Fig. 7 XPS spectra of metals 2p region: **a** Cu/BEA and Cu/BEA/s. **b** Co/BEA and Co/BEA/s. **c** Fe/BEA and Fe/BEA/s

an absence of Co^{2+} ions in the charge compensation sites. On the TPR profile of Fe-containing BEA three maxima appeared confirming multistep reduction of Fe^{3+} in cations or oxo-cations form [41, 43]. The maximum at 385 °C indicates the reduction of $Fe^{3+} \rightarrow Fe^{2+}$ (Fe_2O_3 in Fe_3O_4) while two other maxima at 550 °C and 610 °C are due to reduction of $Fe_3O_4 \rightarrow FeO \rightarrow Fe^0$. [43] It should be pointed that in the case of the Fe/BEA/s sample the reduction maxima on the TPR profile are slightly shifted towards higher temperatures indicating that Fe species in this case are less reducible.

The XPS spectra of Cu 2p, Co 2p and Fe 2p regions are shown in Fig. 7. They reveal that the added metals are in oxidized or hydrated forms. The catalysts prepared by sonication contain metal species in more different forms than prepared by the ion-exchange method. The XPS results confirm the presented previously results concerning oxidation state of metals in the BEA framework and also suggest higher dispersion of active metal phase inside the zeolite matrix. The main peaks of Cu $2p_{3/2}$, located at 933.9 eV for Cu/BEA and slightly shifted in the case of sonicated Cu/BEA/s at 934.2 eV, are connected with M–O binding. The clear shoulders observed at higher binding energies suggest significant hydroxylation of the surface. In the case Co-containing catalysts, the main Co $2p_{3/2}$ peak is at 783.7 and 783.3 eV, typical of Co–O bindings, for Co/BEA and Co/BEA/s, respectively. The binding energies of photoemission observed in the Fe $2p_{3/2}$ region for Fe/BEA and Fe/BEA/s are 712.2 and 712.5 eV, respectively, and are associated with iron oxides.

Following the observed experimentally oligomeric [M–O–M] species, we developed a theoretical model of BEA zeolite (Fig. 1a). The stabilization of dimeric M–O–M complexes (where M = Co, Cu or Fe) in the BEA cluster was investigated. Dimeric models used previously in studies of isocyanic acid adsorption were used: metals adsorbed above zeolitic oxygen bound to Al and bridged by additional oxygen [44]. As a next step the LA adsorption and formation of AA have been considered. The dehydration of LA into

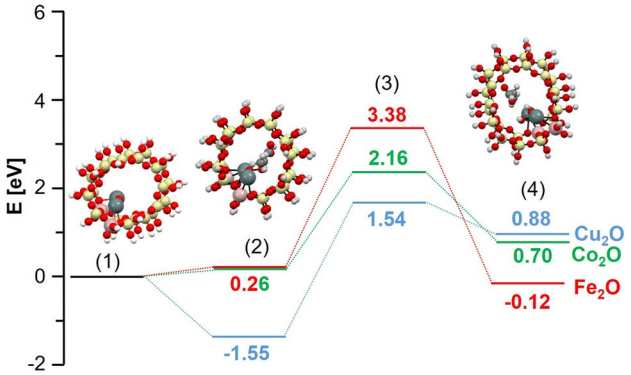

Fig. 8 Energy diagram of lactic acid dehydration into acrylic acid over dimeric M–O–M complex in the BEA zeolite, where M = Co (green), Cu (blue) or Fe (red). Energy level of (1) M–O–M dimer, (2) lactic acid adsorption, (3) transition state, (4) acrylic acid desorption over metal dimer

AA requires the subtraction of hydrogen from the β-carbon (methyl group) and the hydroxyl group from the α-carbon (Fig. 1b). The LA molecule has three available atoms for adsorption above the catalyst surface: the oxygen atom of the hydroxyl group from α-carbon and the two oxygen atoms of the carboxyl group. Based on the literature [45], LA adsorption on zirconia oxide gives several possible binding modes: monodentate, bidentate bridging and bidentate chelating. We attempted to find a path of LA dehydration inside the pure and metal substituted zeolite framework. Therefore, possible modes of interaction of LA with different cations (Si, Al, Co, Cu and Fe) inside the zeolite framework were considered. However, it was shown that the LA did not interact with the zeolite framework sites.

Consequently, another direct pathway of LA dehydration was verified, which involves the simultaneous interaction of hydrogen from the β-carbon (methyl group) and the hydroxyl group from the α-carbon. The possibility of direct LA dehydration, reported in the literature [46], is the interaction of

Table 2 Catalytic performances of BEA catalysts

Catalysts	LA conv.%	Time of process h	Product selectivity %								AA yield%
			AA	AD	PA	AC	2,3-PD	1,2-PD	LAC	Others	
Na/BEA 12.5	96.8	1	0.1	30.8	1.0	1.6	6.5	–	–	60.1	0.1
	99.9	2	–	65.1	0.9	1.7	7.4	–	–	24.9	–
	99.6	3	–	68.2	0.8	1.9	9.1	–	–	20.0	–
	99.8	4	–	52.4	–	0.6	16.9	–	–	30.1	–
	99.5	5	–	39.8	–	–	13.8	–	–	46.4	–
Na/BEA 37.5	96.9	1	0.2	30.7	1.1	1.4	6.3	–	–	60.5	0.1
	99.5	2	–	65.5	0.8	1.8	7.2	–	–	24.7	–
	99.5	3	–	68.4	0.9	1.8	9.0	–	–	19.9	–
	99.4	4	–	52.6	–	0.4	16.9	–	–	30.1	–
	99.0	5	–	39.4	–	–	14.0	–	–	46.6	–
Cu/BEA 12.5	89.9	1	0.5	32.9	3.5	1.8	9.7	–	0.7	51.5	0.4
	97.5	2	0.8	70.9	4.3	2.1	10.8	–	0.8	10.3	0.8
	98.5	3	3.5	66.4	10.8	3.6	12.3	–	0.5	2.9	3.5
	99.8	4	–	72.2	1.4	–	1.9	–	0.2	23.6	–
	100	5	–	78.5	–	–	14.8	–	–	6.7	–
Cu/BEA 37.5	89.7	1	0.3	32.8	3.6	1.8	9.7	–	0.8	51.0	0.2
	97.1	2	0.4	70.7	4.6	2.1	11.0	–	0.7	10.5	0.4
	98.8	3	3.1	66.8	10.5	3.9	12.1	–	0.4	3.2	3.1
	99.1	4	–	72.2	1.6	–	2.0	–	0.3	23.9	–
	100	5	–	79.0	–	–	14.5	–	–	6.5	–
Cu/BEA/s 12.5	99.8	1	–	74.0	0.8	–	2.8	1.4	–	21.0	–
	99.6	2	34.2	–	17.5	32.4	0.8	–	–	15.1	34.2
	99.8	3	47.4	–	16.1	27.4	–	–	–	9.1	47.4
	99.9	4	42.9	–	26.8	30.3	–	–	–	–	42.9
	99.7	5	62.2	–	8.9	20.6	–	–	–	8.3	62.2
Cu/BEA/s 37.5	99.9	1	–	74.2	0.6	–	2.9	1.0	–	21.3	–
	99.8	2	34.1	–	17.3	32.2	1.0	–	–	15.4	34.1
	99.6	3	47.2	–	16.0	27.6	–	–	–	9.2	47.2
	99.8	4	42.7	–	26.9	30.4	–	–	–	–	42.7
	99.9	5	62.4	–	8.8	20.3	–	–	–	8.5	62.4
Co/BEA 12.5	88.7	1	30.5	17.3	17.5	20.1	3.2	–	3.0	8.4	30.4
	97.9	2	44.7	11.3	10.5	9.4	7.1	–	2.5	14.5	44.5
	87.7	3	38.5	–	8.6	3.2	0.5	–	–	49.2	38.1
	99.4	4	27.4	2.6	14.6	4.8	10.4	–	8.9	31.3	27.2
	99.9	5	13.2	–	48.8	–	38.0	–	–	–	13.2
Co/BEA 37.5	88.8	1	31.5	17.1	17.2	19.8	3.2	–	2.9	8.3	31.4
	98.9	2	45.7	11.1	10.3	9.2	6.9	–	2.6	14.2	45.6
	89.7	3	39.4	–	8.4	3.1	0.6	–	–	48.5	39.2
	99.6	4	28.2	2.4	14.2	4.7	10.1	–	8.7	31.7	28.1
	99.8	5	14.4	–	47.9	–	37.7	–	–	–	14.4
Co/BEA/s 12.5	99.9	1	–	100	–	–	–	–	–	–	–
	96.5	2	11.1	47.7	13.6	20.1	4.1	–	–	3.4	10.2
	96.4	3	55.3	–	16.7	23.7	–	–	–	4.3	54.2
	97.5	4	60.9	–	12.6	16.4	–	–	4.7	5.4	60.4
	98.6	5	34.7		28.7	19.9	–	–	16.6	0.1	34.1

Table 2 (continued)

Catalysts	LA conv.%	Time of process h	Product selectivity %								AA yield%
			AA	AD	PA	AC	2,3-PD	1,2-PD	LAC	Others	
Co/BEA/s 37.5	100	1	–	100	–	–	–	–	–	–	–
	96.6	2	11.4	47.3	13.7	20.3	3.8	–	–	3.5	11.4
	96.6	3	57.5	–	16.6	21.3	–	–	–	4.6	55.5
	97.3	4	61.9	–	12.3	16.1	–	–	4.5	5.2	61.9
	98.4	5	35.5		28.1	19.8	–	–	16.4	0.2	35.5
Fe/BEA 37.5	79.4	1	–	22.9	48.8	–	–	–	1.6	26.7	–
	94.8	2	–	32.2	23.7	3.8	7.1	–	–	33.2	–
	95.3	3	4.4	39.4	19.0	10.7	7.6	–	–	18.9	4.4
	96.2	4	2.6	46.2	28.4	8.7	–	–	–	14.1	2.6
	100	5	–	100.0	–	–	–	–	–	–	–
Fe/BEA/s 37.5	76.0	1	–	–	3.3	4.4	–	–	3.6	88.7	–
	95.2	2	10.2	–	50.8	16.4	–	–	0.3	22.3	10.2
	95.7	3	15.4	–	65.1	7.3	0.2	0.3	0.2	11.5	15.4
	94.1	4	10.2	–	68.2	5.4	0.2	–	0.9	15.1	10.2
	100	5	–	–	100	–	–	–	–	–	–

AA acrylic acid, *AD* acetaldehyde, *PA* propionic acid, *AC* acetic acid, *2,3-PD* 2,3-pentanedione, *1,2-PD* 1,2-propanediol, *LAC* lactide

LA with water, where water takes part in the transition state of the dehydration reaction by forming a six-member ring transition state (binding via the oxygen atom with the hydroxyl group from the LA–α-carbon and via the hydroxyl group ith the hydrogen from the LA–β-carbon). The metal dimers have similar potential for the direct LA dehydration. Additionally, the size of BEA pores are enough large for LA dehydration. As is demonstrated in Fig. 1c, d, the topology of metal dimers inside a BEA pore allows to LA adsorption, rotation and dehydration. Through the analysis of geometric compatibility, the metallic dimers, M–O–M, have been considered for the formation of the transition state between LA and AA, based on previous studies of iron dimers inside zeolite [32]. The adsorption of LA was investigated based on the Co–, Cu– and Fe–BEA cluster models. Figure 8 shows the energy diagrams of the dehydration of LA into AA over dimeric metal complexes inside a pore of BEA zeolite. The structure of LA molecule, adsorbed at the M–O_B–M dimer inside the BEA pore is shown in Figs. 1c and 8 (2). The distance between the oxygen center of the LA–α-carbon hydroxyl group and the LA–β-carbon hydrogen is 2.63 Å (see Fig. 1b), which is favorable in terms of the geometrical compatibility with the M–O distance, which equals 1.67 Å in average for all investigated metal dimers. The distance between the LA–β-carbon hydrogen and the bridge oxygen of M–O_b–M dimer is still too long to allow for the hydrogen subtraction from LA and the formation of hydroxyl group. The electronic properties of the metal dimer show that the bridge oxygen starts interacting weakly with the LA–β-carbon hydrogen. Therefore, in the second step the transition state is considered (Fig. 8 (3)), where the adsorbed LA molecule rotates and the LA–β-carbon hydrogen bond is shortened. The metal center binds with the hydroxyl group from the LA–α-carbon and the bridge oxygen with hydrogen from the LA–β-carbon. The adsorption of LA is endothermic in the case of Co– and Fe–BEA (both 0.26 eV), and exothermic (− 1.55 eV) for the Cu–BEA catalyst (Fig. 8 (2)). The dehydration of LA into AA proceeds with energy barriers of 2.16, 1.54 and 3.38 eV inside pores of Co–, Cu– and Fe–BEA (Fig. 8 (3)), respectively. After desorption of AA, two strong OH groups remain at the M–O_b–M dimer. The lowest energy barrier is observed in the case of copper. Therefore, the Cu–BEA catalyst should be the most promising for the AA production.

The tests of catalytic performance confirms trends in the AA formation postulated theoretically. We investigated different metal exchanged zeolites (with various metals such as Na, Sn, Zn, Fe, Co, Cu) for the LA to AA reaction. The data presented in Table 2 were collected in the dehydration reaction of LA to produce AA over Na–BEA as delivered and the Co–, Cu– and Fe–BEA zeolites, prepared using the ion exchange and sonication methods. The formation of following byproducts was detected in the catalytic tests: AA, propionic acid, 2,3-pentanedione, acetaldehyde, and 1,2-propanediol. The Na–BEA and Fe/BEA catalysts showed mainly activity towards acetaldehyde. Additionally, the production of acetaldehyde is not correlated with a number of acidic sites, as is shown in Fig. 9a. The best activity in the formation of AA was achieved over the Co– and Cu–BEA catalysts. The sonicated Co– and Cu–BEA zeolites were found

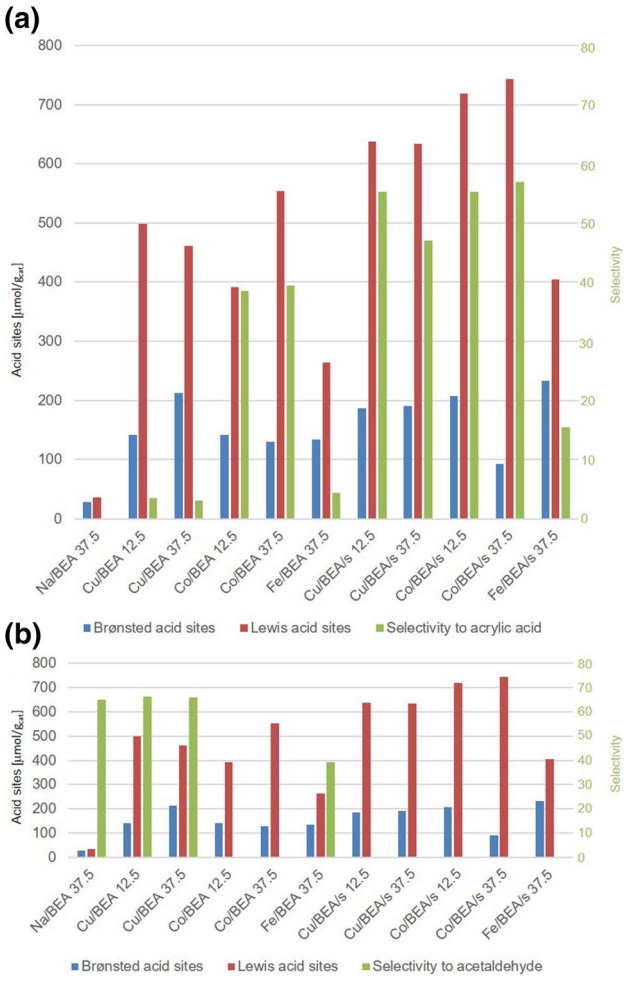

Fig. 9 Correlation of performance of BEA catalysts in conversion of lactic acid after 3 h of process in function of acidic sites: **a** selectivity to acetaldehyde, **b** selectivity to acrylic acid

to catalyze the dehydration of LA into AA with the highest selectivity to AA. The production of AA over the sonicated Co/BEA/s and Cu/BEA/s catalysts increases with the time of process. It must be also pointed out, that the structure of the catalysts prepared by the sonochemical method differs from that for the materials prepared by conventional ion exchange. The concentration of Lewis active sites in the catalysts prepared by the sonochemical route almost doubles in comparison with the catalysts modified with the ion-exchange method (cf. Table 1). This may be connected with the favorable formation of the metal/metal oxide nanoparticles during the sonochemical irradiation process and/or higher dispersion of active phase onto the zeolite matrix. Interestingly, the concentration of Lewis sites only slightly changes with the change of Si/Al ratio. The results of the carbon monoxide chemisorption studies and in situ UV–Vis suggest, that the better selectivity of catalyst prepared by the sonochemical route may be connected with the presence of acid Lewis sites in the form of metal oligomeric species. The importance of Lewis sites for the LA dehydration are also confirmed by limitation of this reaction in the case of Na/BEA, where the low amount of Lewis sites is available. Lari et al. found a high selectivity to AA over a NaY catalyst [18]. However, in that case an amount of Na was much more higher and they studied hierarchical zeolites. Figure 9a shows selectivity of the LA dehydration into AA after 3 h in comparison with selectivity to acetaldehyde (Fig. 9b). The Si/Al ratio of the Cu– and Co–BEA catalysts has negligible influence on selectivity to AA. The selectivity of LA dehydration into AA correlates strongly with an increase of concentration of acidic sites, mainly Lewis sites. In the case of Co/BEA/s the conversion into AA highly decreases after 4 h of the process and more propionic acid is formed. The best performance with selectivity ca. 62% was achieved in the presence of the Cu/BEA/s (both, with Si/Al 12.5 and 37.5) catalyst after 5 h with relatively low amount of other products, such as acetic acid (20%), propionic acid (9%) and others (8%). These results are compatible with performances obtained in LA dehydration towards AA over ZSM-5 catalysts [40]. However, Zhang et al. used the hierarchical ZSM-5 zeolites. Cu/BEA/s contains the highest amount of Cu-metal in zeolite framework as well as the oligomeric [Cu^{2+}–O^{2-}–Cu^{2+}] species. As shown by our theoretical and experimental results, the amount of oligomeric [Cu^{2+}–O^{2-}–Cu^{2+}] species is essential for the direct LA dehydration into AA. Therefore, according to our finding using the sonicated Cu–BEA catalyst, in a next step of investigation hierarchical BEA zeolites with sonicated Co and Cu species will be prepared. In our opinion, the hierarchization process should improve the performance of our Cu/BEA/s catalysts.

4 Conclusions

In summary, from an energetics point of view, the Co– and Cu–BEA zeolites have the best catalytic properties for the direct dehydration of LA into AA above dimeric M–O–M species present inside a zeolite pore. A similar reaction mechanism is also expected at the polymeric metal species, where the series of bridge oxygen are present. The theoretical prediction of catalyst activity agrees with the results of catalytic tests in gaseous phase, where sonicated catalysts, Co/BEA/s and Cu/BEA/s, have the best selectivity into AA (above 60%). The sonicated catalysts show improved oligomeric [M–O–M] species distribution, which is essential for selectivity to AA. However, co-existence of other active sites succeeds in formation of other byproducts like propionic acid, 2,3-pentanedione or acetaldehyde. Time of proceeding catalytic process is also important. The best results were obtained after 3–5 h of the dehydration process.

Acknowledgements This article is the effect of realization of project "Nano-design of zeolite-based catalysts for selective conversion of biomass into chemicals" sponsored by National Science Centre, Poland under Polonez-1 Grant No. 2015/19/P/ST4/02482. This project has received funding from the European Union's Horizon 2020 research and innovation programme under the Marie Skłodowska-Curie grant Agreement No. 665778. The theoretical work was supported also in part by the PL-Grid Infrastructure. The sonicated catalysts has been prepared as an effect of realization of Project No. 2015/17/D/ST8/01252 sponsored by National Science Centre, Poland.

Open Access This article is distributed under the terms of the Creative Commons Attribution 4.0 International License (http://creativecommons.org/licenses/by/4.0/), which permits unrestricted use, distribution, and reproduction in any medium, provided you give appropriate credit to the original author(s) and the source, provide a link to the Creative Commons license, and indicate if changes were made.

References

1. Pacala S, Socolow R (2004) Science 305:968–972
2. Werpy T, Petersen G (2004) Top value added chemicals from biomass, Vol. I-results of screening for potential candidates from sugars and synthesis gas, Report No. NREL/TP-510-35523, National Renewable Energy Laboratory, Golden, CO
3. Huber W, Iborra S, Corma A (2006) Chem Rev 106:4044–4098
4. Langan P, Gnanakaran S, Rector KD, Pawley N, Fox DT, Cho DW, Hammel KE (2011) Energy Environ Sci 4:3820–3833
5. da CostaSousa L, Chundawat SPS, Balan V, Dale BE (2009) Curr Opin Biotechnol 20:339–347
6. Himmel ME, Ding SY, Johnson DK, Adney WS, Nimlos MR, Brady JW, Foust TD (2007) Science 315:804
7. Hammaecher C, Paul J-F (2013) J Catal 300:174–182
8. Corma A, Iborra S, Velty A (2007) Chem Rev 107:2411–2502
9. Stöcker M (2008) Angew Chem Int Ed Engl 47:9200–9211
10. Mäki-Arvela P, Simakova I, Salmi T, Murzin DY (2014) Chem Rev 114:1909–1971
11. https://mcgroup.co.uk/news/20140508/china-leads-acrylic-acid-market-terms-production-consumption.html. Accessed 22 Aug 2018
12. Rinaldi R, Schüth F (2009) Energy Environ Sci 2:610–626
13. Sun P, Yu D, Fu K, Gu M, Wang Y, Huang H, Ying H (2009) Catal Commun 10:1345–1349
14. Yu D, Sun P, Tang Z, Li Z, Huang H (2011) Can J Chem Eng 89:484–490
15. Yan J, Yu D, Li H, Sun P, Huang H (2010) J Rare Earths 28:803–806
16. Sun P, Yu D, Tang Z, Li H, Huang H (2010) Ind Eng Chem Resour 49:9082–9087
17. Sazama P, Pilar R, Mokrzycki L, Vondrova A, Kaucky D, Plsek J, Sklenak S, Stastny P, Klein P (2016) Appl Catal B 189:65–74
18. Lari GM, Puértolas B, Frei MS, Mondelli C, Pérez-Ramírez J (2016) ChemCatChem 8:1507–1514
19. Bonnotte T, Paul S, Araque M, Wojcieszak R, Dumeignil F, Katryniok B (2018) Chembioeng Rev 5:34–56
20. Milina M, Mitchell S, Crivelli P, Cooke D, Pérez-Ramírez J (2014) Nat Commun 5:4922
21. Zhang XQ, Trinh TT, van Santen RA, Jansen APJ (2011) J Am Chem Soc 133:6613–6625
22. Szyja BM, Hensen EJM, van Santen RA (2011) Catal Today 169:156–166
23. Yang G, Pidko E, Hensen EJM (2013) J Phys Chem C 117:3976–3986
24. Lisboa O, Sanchez M, Ruette F (2008) J Mol Catal A 294:93–101
25. Malola S, Svelle S, Bleken FL, Swang O (2012) Angew Chem Int Ed 51:652–655
26. Fjermestad T, Svelle S, Swang O (2013) J Phys Chem C 117:13442–13451
27. Silaghi MC, Chizallet C, Raybaud P (2014) Microporous Mesoporous Mater 191:82–96
28. Czekaj I, Brandenberger S, Kröcher O (2013) Microporous Mesoporous Mater 169:97–102
29. Rutkowska M, Piwowarska Z, Micek E, Chmielarz L (2015) Microporous Mesoporous Mater 209:54–65
30. Castilho S, Borrego A, Henriques C et al (2017) Inorg Chim Acta 455:568–574
31. Chlebda DK, Stachurska P, Jędrzejczyk RJ et al (2018) Nanomaterials 8:21
32. Pérez-Ramírez J, Groen JC, Brückner A, Kumar MS, Bentrup U, Debbagh MN, Villaescusa LA (2005) J Catal 232:318–334
33. International Zeolite Association (2018) Database of Zeolite Structures, (n.d.). http://www.iza-structure.org/databases/. Accessed 5 July 2018
34. Ohtsuka H, Tabata T, Okada O, Sabatino LMF, Bellussi G (1998) Catal Today 42:45–50
35. Mihailova B, Valtchev V, Mintova S, Faust A-C, Petkova N, Bein T (2005) Phys Chem Chem Phys 7:2756–2763
36. M. Rashad, M. Rüsing, G. Berth, K. Lischka, and A. Pawlis, J. of Nanomaterials 2013, Article ID 714853, 6 pages
37. Deng Y, Handoko AD, Du Y, Xi S, Yeo BS (2016) ACS Catal 6:2473–2481
38. Chlebda DK, Jędrzejczyk RJ, Jodłowski PJ, Łojewska J (2017) J Raman Spectrosc 2017:48
39. Chamritski I, Burns G (2005) J Phys Chem B 109:4965–4968
40. Li J, Wilken N, Kamasamudram K, Currier NW, Olsson L, Yezerets A (2013) Top Catal 56:201–204
41. Liu N, Zhang R, Chen B, Li Y, Li Y (2012) J Catal 294:99–112
42. Essid S, Ayari F, Bulánek R, Vaculík J, Mhamdi M, Delahay G, Ghorbel A (2018) Catal Today 304:103–111
43. Mauvezin M, Delahay G, Coq B, Kieger S, Jumas JC, Olivier-Fourcade J (2001) J Phys Chem B 105:928–935
44. Dai C, Lei Z, Wang Y, Zhang R, Chen B (2013) Microporous Mesoporous Mater 167:254–266
45. Aida TM, Ikarashi A, Saito Y, Watanabe M, Smith RL Jr, Arai K (2009) J Supercrit Fluids 50(3):257–264
46. Zhang X, Lin L, Zhang T, Liu H, Zhang X (2016) Chem Eng J 284:934–941

Publisher's Note Springer Nature remains neutral with regard to jurisdictional claims in published maps and institutional affiliations.